

Article

Adsorption Performance and Mechanism of H₃PO₄-Modified Banana Peel Hydrothermal Carbon on Pb(II)

Tao Bai ^{1,*}, Yuhu Yao ¹, Jiaxin Zhao ¹, Laixin Tian ^{1,2} and Luming Zhang ¹

¹ School of Electric Power, Civil Engineering and Architecture, Shanxi University, Taiyuan 030006, China; 202123504022@email.sxu.edu.cn (Y.Y.); 202223505016@email.sxu.edu.cn (J.Z.); comtianlaixin@geg.com.cn (L.T.); 202223505014@email.sxu.edu.cn (L.Z.)

² Guangdong Energy Group, Taiyuan 030006, China

* Correspondence: hdbaitao@sxu.edu.cn

Abstract: This study investigated the adsorption performance of hydrothermal carbon derived from banana peel and modified with different concentrations of phosphoric acid solution, then used to adsorb lead ions in an aqueous solution. The surface structure and functional groups of the modified hydrothermal carbon were analyzed using XRD, SEM, FT-IR, elemental analysis, and BET. The results showed that the adsorption capacity of modified hydrothermal carbon derived from banana peel reached 40.64 mg/g at a hydrothermal temperature of 240 °C, a phosphoric acid solution of 2 mol/L, and a solid–liquid ratio of 2 g/L, with a removal efficiency of 82.74%. The adsorption process conformed to the pseudo-second-order kinetic model and the Langmuir isotherm equation. The correlation coefficient of 0.99 for fitting the adsorption process using an artificial neural network, indicating that the artificial neural network could be used to predict adsorption. The adsorption of Pb(II) from an aqueous solution by phosphoric acid-modified hydrothermal carbon was dominated by monolayer chemical adsorption, and the adsorption mechanisms included electrostatic attraction, ion exchange, surface complexation, and physical adsorption.

Keywords: hydrothermal carbon; modification; adsorption; lead ion; mechanism



Citation: Bai, T.; Yao, Y.; Zhao, J.; Tian, L.; Zhang, L. Adsorption Performance and Mechanism of H₃PO₄-Modified Banana Peel Hydrothermal Carbon on Pb(II). *Separations* **2024**, *11*, 17. <https://doi.org/10.3390/separations11010017>

Academic Editor: Zhiqian Jia

Received: 3 November 2023

Revised: 28 December 2023

Accepted: 28 December 2023

Published: 3 January 2024



Copyright: © 2024 by the authors. Licensee MDPI, Basel, Switzerland. This article is an open access article distributed under the terms and conditions of the Creative Commons Attribution (CC BY) license (<https://creativecommons.org/licenses/by/4.0/>).

1. Introduction

Heavy metals pose great hazards when they enter water bodies, with electroplating, metallurgy, mining, the chemical industry, and processing being the main sources [1]. The direct discharge of industrial wastewater containing heavy metals can greatly damage the human body and destroy the ecological environment [2].

Currently, the most common treatment methods for removal of heavy metals include electroflocculation, electroflotation, chemical precipitation, ion exchange, membrane filtration, photocatalysis, nanotechnology, and adsorption, amongst others [3–9]. By comparison, the technical cost and economic benefits are ranked in order: adsorption > ion exchange > electroflotation > membrane filtration > electroflocculation > chemical precipitation > photocatalysis > nanotechnology. Compared with other technologies, the adsorption method has a wide range of applications and a simple preparation method; therefore, it has many prospective applications [10].

High-temperature adiabatic carbonization and low-temperature hydrothermal carbonization are common methods for biomass carbonization [11], and there are many studies focusing on the preparation of activated carbon with high adsorption performance [12]. The hydrothermal carbonization process is simple [13], and the reacting raw materials do not require drying treatment. The hydrothermal carbon thus prepared is widely used in the adsorption and removal of pollutants [14]. The process of hydrothermal carbonization involves the dehydration and decarboxylation of the functional groups of substances, resulting in an increased carbon content, higher carbon density, and better adsorption performance of the reactants [15]. Additionally, hydrothermal carbon exhibits the high

adsorption of lead and arsenic [16]. Bananas are the world's fifth-largest crop and second-largest fruit, accounting for about 16 percent of the total fruit production worldwide. With the rapid industrialization of China, banana cultivation has been gradually industrialized, and the output has increased rapidly [17], exceeding 12.1 million tons in 2022. Banana peel, a by-product in the processing of banana products (food, beverages, and chemicals), accounts for 30–40% of the total weight of bananas [18] and is a typical biomass waste. Banana peel is an inexpensive adsorbent with a good adsorption capacity for many heavy metals, such as lead, chromium, cadmium, copper, and zinc. However, the adsorption capacity and removal efficiency of raw banana peels are limited. Studies have shown that hydrothermal carbon with a high added value for heavy metal adsorption can be obtained from banana peel using the hydrothermal method [19]. In a previous study, a batch experiment removed Pb(II) through a derived powered adsorbent from the banana peel. Parameters such as pH, dosage, time, and agitating speed were evaluated, and a maximum capacity of 2.18 mg/g was observed after adsorption [20]. The adsorption capacity of lead (II) on biochar prepared from banana peel after acid treatment was increased to 20.97 mg/g [21]. Banana peel biochar was also modified and used to remove As(V), and the maximum adsorption capacity was found to be 1.04 mg/g [22].

Modification is an effective means by which to change the surface activity of hydrothermal carbon in order to further improve its adsorption performance. There are few studies on the surface modification of banana peel hydrothermal carbon done to improve functional groups and promote surface affinity [23].

Based on this past work, this study attempts to prepare modified hydrothermal carbon from banana peel as an adsorption material in a reaction kettle under different phosphoric acid solutions at 240 °C. The aim of this work is to study the influence of hydrothermal carbon on the removal of lead ions in solution under different phosphoric acid solutions, pH values, solid–liquid ratios, and adsorption times and to analyze the surface morphology of the hydrothermal carbon using XRD, SEM, FTIR, BET, and elemental analysis to investigate the adsorption mechanism. This work aims to provide basic data and a theoretical basis for the industrial application of the preparation of hydrothermal carbon modified by a phosphoric acid solution to remove lead ions from solution.

2. Materials and Methods

2.1. Raw Materials

Banana peel was purchased from the food market in Taiyuan.

2.2. Reagents

The phosphoric acid (H₃PO₄) used is an analytical-grade reagent from Shanghai Maclean's Biochemical Technology Co., Ltd. (Shanghai, China). The hydrochloric acid is of analytical grade, and it was provided by China Pharmaceutical Group Chemical Reagent Co., Ltd. (Shanghai, China). A total of 1000 mg/L of a lead standard solution was provided by Shanghai Maclean's Biochemical Technology Co., Ltd.

2.3. Experimental Methods

2.3.1. Preparation of Hydrothermal Carbon from Banana Peel

The banana peel purchased in the market was washed with tap water, placed in a 105 °C drying oven to achieve a constant weight, and then crushed over an 80-mesh standard sample screen. The hydrothermal carbonization process was carried out in an N₂ atmosphere. The temperature rose from room temperature to 240 °C at 10 °C/min, and the heat was maintained for 120 min. After it was allowed to cool naturally to room temperature, the hydrothermal product was placed in a drying oven until a constant weight was achieved. Then, secondary grinding was carried out to obtain hydrothermal carbon made from banana peel with a particle size below 70 mesh. The hydrothermal carbon prepared at 240 °C was labeled HTC240.

2.3.2. Preparation of Phosphoric Acid-Modified Hydrothermal Carbon

Phosphoric acid solutions of different concentrations (1.0 mol/L, 1.5 mol/L, 2.0 mol/L, and 3.0 mol/L) were mixed with banana peel, soaked in a constant-temperature water bath oscillator (45 °C, 200 rpm) for 6 h, and then placed in a hydrothermal reactor for hydrothermal carbonization under N₂. The temperature rose from room temperature to 240 °C at 10 °C/min, and the heat was maintained for 120 min. After it was allowed to cool naturally to room temperature, the hydrothermal product was placed in a drying oven until a constant weight was achieved. Secondary grinding was then carried out to obtain modified hydrothermal carbon with a particle size below 70 mesh. The prepared hydrothermal carbons were labeled P-HTC-1.0, P-HTC-1.5, P-HTC-2.0, and P-HTC-3.0, respectively, according to the concentration of the modified phosphoric acid solution.

2.3.3. Adsorption Experiment

Ultra-pure water was added to the lead standard liquid. Then, it was diluted into 50 mg/L, 100 mg/L, 400 mg/L, and other lead-ion reserve liquids. A specific amount of hydrothermal carbon was added to the lead solution, aiming to maintain a specific solid-to-liquid ratio, and then the adsorption experiment was carried out in a constant-temperature water-bath oscillator. After shaking, the supernatant was allowed to stand, then 10 mL was removed from the centrifuge tube. After centrifugation, the absorbance of the supernatant was measured by spectrophotometry. According to the standard curve generated for the lead solution, the adsorption capacity and removal efficiency of hydrothermal carbon were calculated according to Formulas (1) and (2). All the experiments were conducted in triplicate, and the results presented are the average values of the three experiments.

$$q_e = ((C_0 - C_{e,t}) \times V) / m \quad (1)$$

$$\eta = (C_0 - C_{e,t}) / C_0 \times 100\% \quad (2)$$

where q_e is the adsorption capacity, mg/g; η is the removal rate as a %; C_0 and $C_{e,t}$ are, respectively, the initial and post-adsorption concentrations of the lead solution in mg/L; V is the volume of the solution in L; and m is the mass of modified hydrothermal carbon in g.

2.3.4. Experimental Equipment

The pH value of the solution was determined using a PHSJ-3F pH meter (precision 0.1, Shanghai Yidian Scientific Instrument Co., Ltd. (Shanghai, China)). The concentration of lead in the solution was determined using a P4 UV-visible spectrophotometer (Shanghai Meppan Instrument Co., Ltd. (Shanghai, China)). A TESCANMIRALMS scanning electron microscope (Tesken (China) Co., Ltd. (Shanghai, China)) was used to obtain the surface morphology of the hydrothermal carbon before and after modification. The accelerated voltage was 10 kV. The properties of the hydrothermal carbon surface before and after modification were analyzed using an Empyrean X-ray diffractometer (Malvern Instruments China Co., Ltd. (Shanghai, China)). The pore structure of the hydrothermal carbon was measured by BET using a Micromeritics ASAP 2460 automated specific surface and porosity analyzer. The elemental content of the hydrothermal carbon was determined using an elemental analyzer (Elementar Vario EL). The main functional groups of the Fourier transform were obtained from the samples collected by the Nicolet IS20 infrared spectrometer (Somerset Fisher Technology (China) Co., Ltd. (Shanghai, China)) to further determine the material's structure.

3. Results

3.1. Surface Structure and Properties of Hydrothermal Carbon before and after Modification

3.1.1. SEM Analysis

Figure 1 shows the SEM images of hydrothermal carbon before and after modification. As can be seen from Figure 1a, the surface of the unmodified hydrothermal carbon is smooth, and there are fewer carbon microspheres compared to the modified structure. As

shown in Figure 1b, many carbon microspheres of different sizes are present on the surface of the modified hydrothermal carbon. The smaller carbon particles are more numerous, and their diameters are only tens of nanometers. Thus, surface pores are formed [24]. Many gases, such as CO₂ and C_xH_y, are generated. These gases change the structure of the carbon skeleton and form pores of different sizes and structures [25].

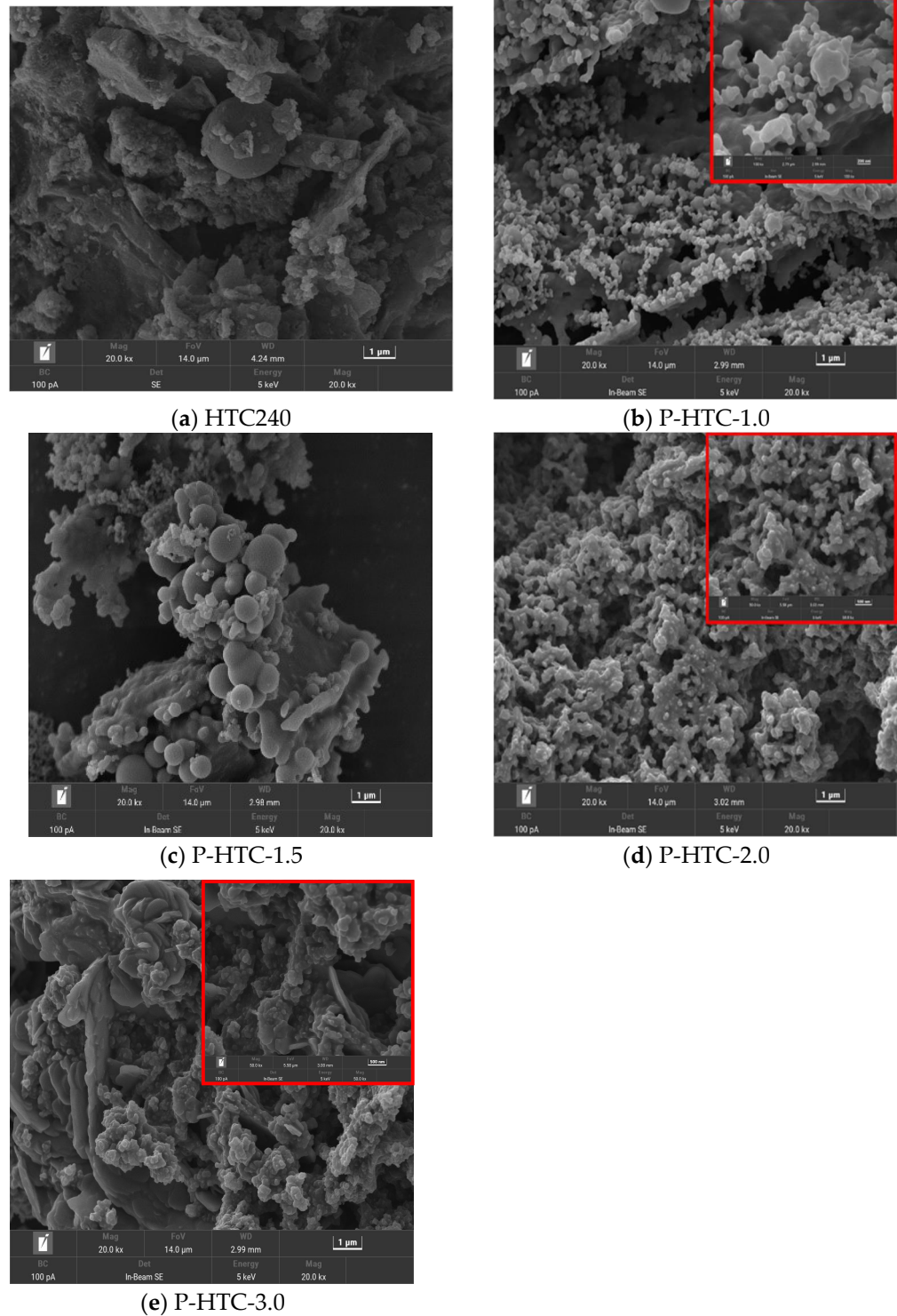


Figure 1. SEM diagram of hydrothermal carbon surface before and after phosphoric acid modification.

As shown in Figure 1c, when the phosphoric acid concentration is increased to 1.5 mol/L, the surface microspheres are larger and most microspheres measure 2–3 μm in

diameter. As shown in Figure 1d, with the increase in the phosphoric acid concentration, the etching in the hydrothermal reaction gradually increases, the surface of the hydrothermal carbon becomes rough and uneven, and the surface porosity increases. As shown in Figure 1e, as the concentration continues to increase, the size of the surface pores decreases. It is deduced that the internal pore structure of hydrothermal carbon begins to collapse and that the structure begins to be destroyed. This change occurs due to the fact that the high concentration of phosphoric acid causes insoluble fatty acids to adhere to the hydrothermal carbon, so a large number of hydrothermal carbons are unable to participate in the reaction. The change may also be caused by the extensive destruction of the pore structure caused by a large amount of gas.

3.1.2. FT-IR Analysis

Figure 2 shows the FT-IR diagram of the hydrothermal carbon before and after modification. It can be seen from the figure that most of the functional groups that are present on the surface of the modified hydrothermal carbon before modification are retained, but there are also vibration peaks in different positions after modification. In the functional-group region, the vibration peaks on the surface of the hydrothermal carbon at 2921 cm^{-1} and 2851 cm^{-1} before and after modification are attributed to aliphatic C-H stretching vibration. There are no obvious absorption peaks attributable to triple-bonded compounds appearing in the range of $2500\sim 2000\text{ cm}^{-1}$. The absorption peak at 1719 cm^{-1} is the result of the vibration of the C=O in carboxyl groups, aldehydes, ketones, and esters. The vibrational peak of C-O/C-O-C at 1000 cm^{-1} indicates that the hydrothermal carbon surface contains a large number of oxygen-containing functional groups. Most of these groups are hydrophilic functional groups, which are conducive to the dispersion of hydrothermal carbon in aqueous solutions and provide more active sites for chemical reactions [26]. The vibration of C=C at 1650 cm^{-1} may be attributed to the formation of carbon-carbon single and double bonds in small molecules generated by hydrolysis during hydrothermal reactions that occur during dehydration, condensation, and aromatization, which in turn generate aromatic compounds [27].

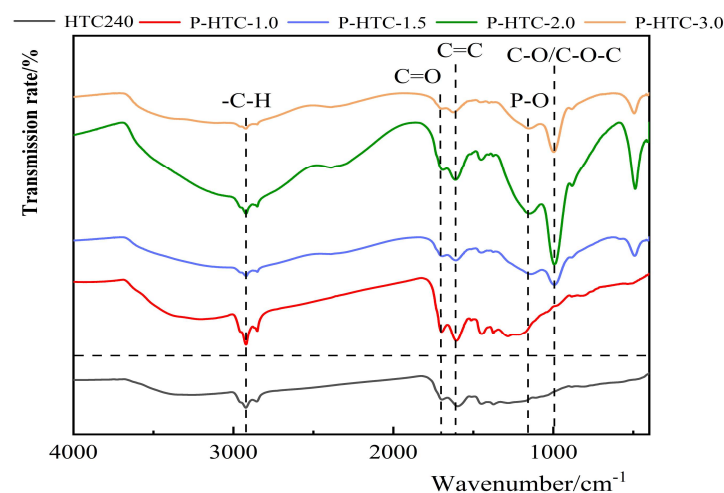


Figure 2. FT-IR diagram of hydrothermal carbon before and after phosphoric acid modification.

With the increase in concentration of the phosphoric acid solution, the C=C, C=O and O/C or C-O-C stretching vibration first increased and then decreased. The maximum stretching vibration, which was achieved at a phosphoric acid concentration of 2 mol/L, was significantly stronger than that of the unmodified hydrothermal carbon. This result indicates that a large number of oxygen-containing functional groups were added to the surface of the modified hydrothermal carbon. This change significantly increases the adsorption of Pb(II) and is one of the most important reasons why hydrothermal carbon

can act as an adsorbent. A strong stretching vibration peak appears at 1100 cm^{-1} for the unmodified material, but it does not appear on the surface of the modified hydrothermal carbon. This peak is identified as the characteristic peak of P-O, indicating that there are more phosphoric acid ions on the surface of the modified hydrothermal carbon. These ions can react with Pb(II) and improve the rate of lead removal [28].

3.1.3. XRD Analysis

Figure 3 shows the XRD pattern of the hydrothermal carbon surface before and after modification. As can be seen from the figure, the positions of the peaks remain roughly the same, with characteristic peaks at 28.3° , 40.5° , and 50.2° . When the diffraction angle is about 22.3° or 22.5° , the corresponding peak belongs to the characteristic peak No. 002 of graphite, indicating that with an increase in the phosphoric acid concentration, the width of the peak gradually increases and the carbonization degree of hydrothermal carbon increases [29]. The appearance of this peak also indicates that the hydrothermal carbon before and after modification is in the form of amorphous carbon, which is suitable for use as adsorbent material [30].

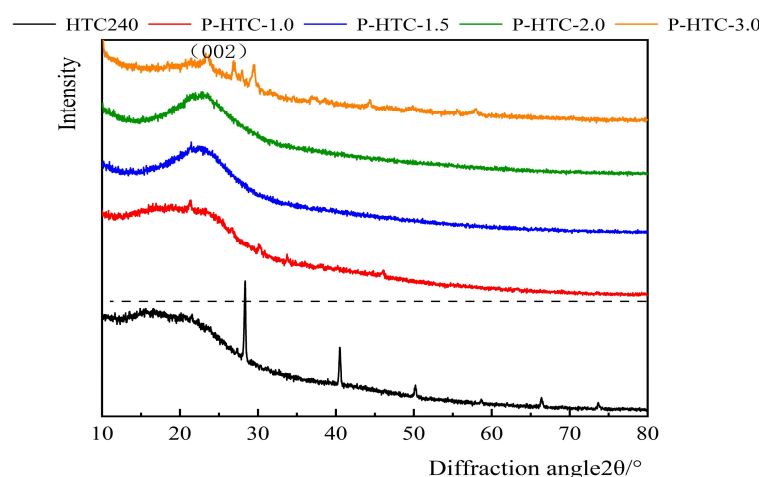


Figure 3. XRD patterns of unmodified hydrothermal carbon and phosphoric acid-modified hydrothermal carbon.

3.1.4. BET Analysis

The specific surface areas of the hydrothermal carbons are shown in Table 1, and the specific surface area of the biomass char was calculated using the BET method. As can be seen from Table 1, after phosphoric-acid activation, the specific surface area of the activated char material decreased and the pore volume and average pore size increased, indicating that phosphoric acid played a pore-making role.

Table 1. Pore-structure parameters of modified hydrothermal carbon.

	BET Surface Area $/(m^2 \cdot g^{-1})$	Total Pore Volume $/(cm^3 \cdot g^{-1})$	Average Pore Size $/nm$
HTC240	7.3709	0.0263	14.2607
P-HTC-2.0	4.6823	0.0339	28.9693

Figure 4 shows the adsorption/desorption curves of hydrothermally treated carbon material derived from banana peel (HTC240) and phosphoric acid-activated carbon material derived from banana peel (P-HTC-2.0). The main reason for the increase in pore space and pore size is that the activation effect of treatment with the phosphoric acid solution during hydrothermal treatment promotes adsorption. However, the corrosive nature of the acid

may also lead to the collapse and interconnection of the pore structure of the hydrothermal carbon, resulting in a decrease in its specific surface area.

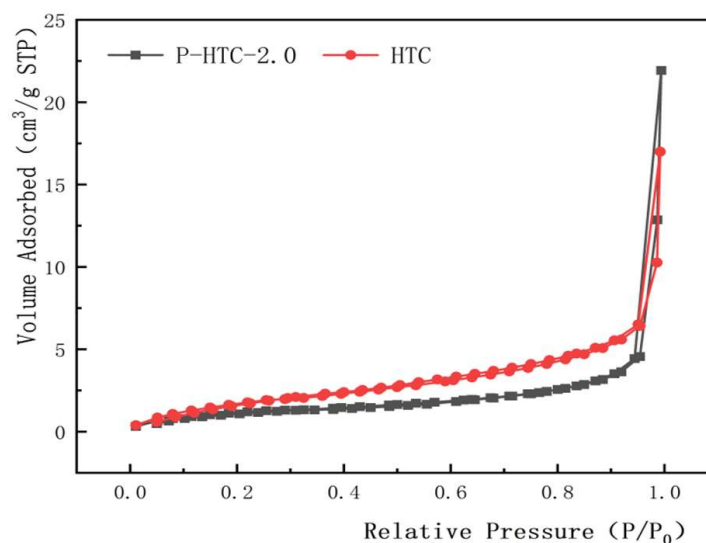


Figure 4. Nitrogen adsorption/desorption curves.

3.1.5. Elemental Analysis

The content of major elements (C, H, O, and N) in the hydrothermal carbon was determined using an elemental analyzer, and the detailed data are shown in Table 2. From the table, it can be seen that the C content of the phosphoric acid-modified hydrothermal carbon decreased slightly, which may be attributed to the fact that treatment with phosphoric acid intensifies the erosion of the carbon structure at high temperatures. It has been shown that phosphoric acid decomposes at high temperatures to produce volatile phosphorus compounds and can oxidize carbon to carbon monoxide, leading to carbon loss. In addition, the O content of the phosphoric acid-modified hydrothermal carbon was higher than that of the unmodified hydrothermal carbon, suggesting that the phosphoric acid modification increased the number of oxygen-containing functional groups on the hydrothermal carbon.

Table 2. Content of C, H, O, and N in hydrothermal carbon.

	C/%	H/%	N/%	O/%
HTC240	69.688	6.229	3.107	15.730
P-HTC-2.0	67.622	6.604	2.847	16.899

3.2. Analysis of the Adsorption Performance of Lead Ions by Modified Hydrothermal Carbon

3.2.1. Influence of Phosphoric Acid Concentration on Lead Adsorption by Hydrothermal Carbon

The experimental conditions were as follows: an adsorption temperature of 25 °C, an initial concentration of lead ions of 50 mg/L, and a solid–liquid ratio of 1 g/L. The experiments were carried out until the adsorption reached equilibrium. The adsorption experiments were carried out on hydrothermal carbon modified using different phosphoric acid solutions. Formulas (1) and (2) were used to calculate the adsorption capacity and yield of the hydrothermal carbon. The calculated results are detailed in Figure 5.

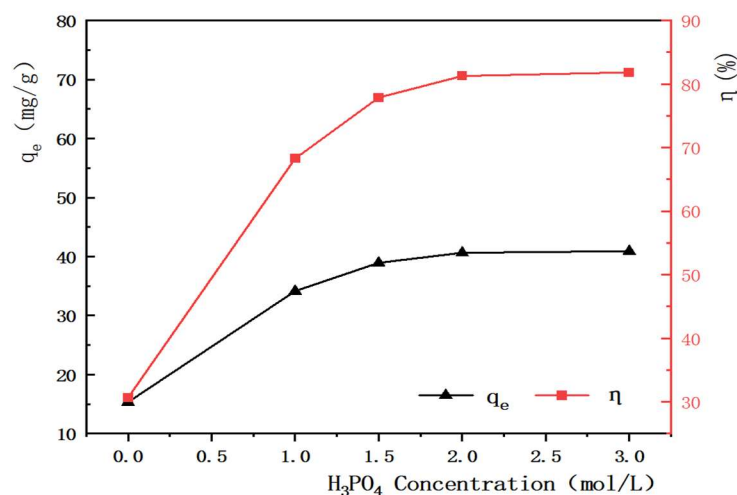


Figure 5. Effect of different phosphoric acid concentrations on adsorption by hydrothermal carbon.

As can be seen from Figure 5, the efficiency of lead removal by modified hydrothermal carbon increases with the increase in the phosphoric acid concentration, and the overall trend shows an initial increase and then stabilization. When the phosphoric acid concentration is 3.0 mol/L, the adsorption capacity of modified hydrothermal carbon reaches 40.65 mg/g, and the removal rate is 81.84%. Compared with the adsorption capacity of 15.32 mg/g and the removal rate of 30.64% before modification, these values increased by 2.6 and 2.7 times, respectively. This change is related to the hydrolysis of cellulose and hemicelluloses in banana peel by phosphoric acid, which results in the formation of many chain molecules that combine with phosphoric acid ions and increase the number of active groups on the surface of the hydrothermal carbon, thus promoting adsorption [31]. In view of the large capacity for lead-ion adsorption of modified hydrothermal carbon generated with an phosphoric acid concentration of 2.0 mol/L, that phosphoric acid concentration is taken as the standard in the following adsorption experiments.

3.2.2. Influence of pH and pHPZC Value on the Adsorption Effect of Lead Ion

A series of 50 mL conical flasks were filled with a 10 mL NaCl solution at a concentration of 0.01 mol/L, and the initial pH of the solution was adjusted to be between 1 and 12. Then, 10 mg of modified material was added to the two groups of conical flasks for comparison, and the pH value of the NaCl solution was determined after filtering out the material after the reaction. The change in pH before and after oscillation was plotted by the initial pH value of the solution. The intersection of the curve and the transverse axis is the zero-potential point of the adsorbent, as shown in Figure 6.

The effects of the pH value on adsorption onto modified hydrothermal carbon are shown in Figure 7. The experimental conditions were as follows: an adsorption temperature of 25 °C, an initial concentration of lead ions of 50 mg/L, a solid–liquid ratio of 1 g/L, a 2 mol/L concentration of the phosphoric acid solution, and a pH value of the solution in the range of 2–7. The reactions were allowed to continue until the adsorption reached equilibrium.

Figure 6 depicts the pHPZC value of the hydrothermal carbon, showing it as the point where the curve intersects the horizontal axis, where the charge on the surface of the material is zero. As the pH range used in this study was between 2 and 7 and was thus always less than 8 (the pHPZC value of hydrothermal carbon), the surface charge of the hydrothermal carbon in this study was obviously always positive.

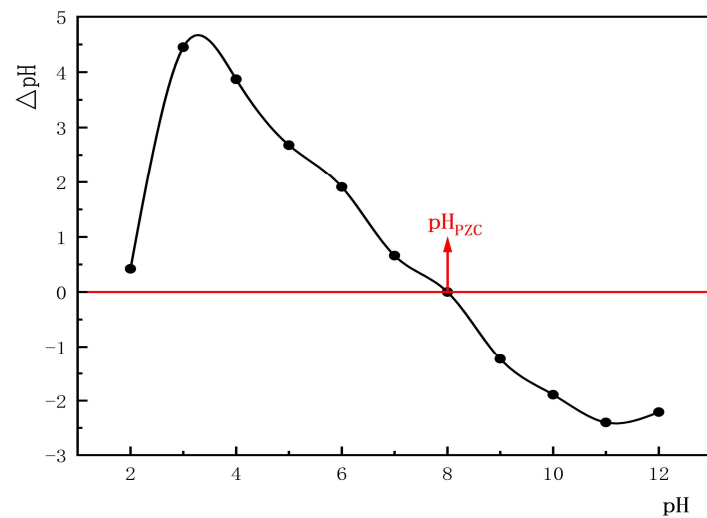


Figure 6. pH_{PZC} of adsorbent.

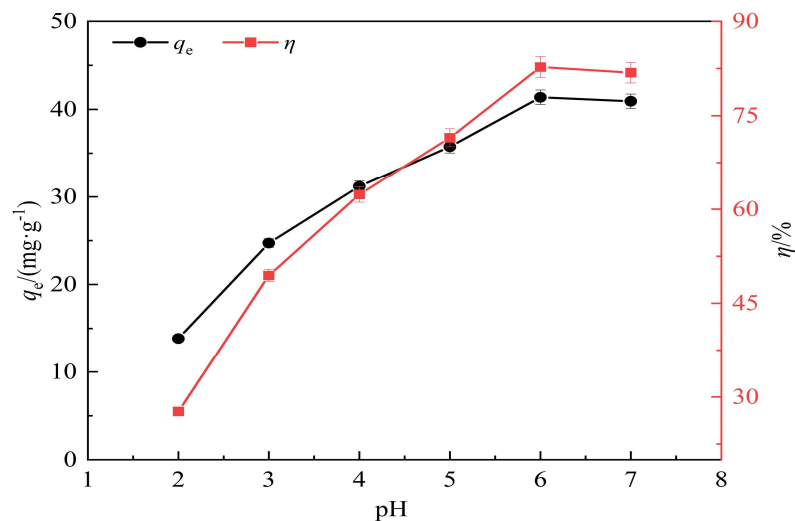
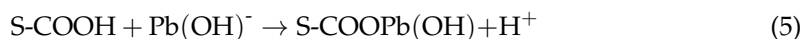
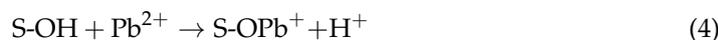
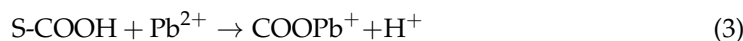


Figure 7. Effect of pH on adsorption of Pb(II) by modified hydrothermal carbon.

As can be seen from Figure 7, in the range of pH values from 2 to 6, the adsorption capacity of modified hydrothermal carbon and the rate of Pb removal rapidly increase with the increase in the solution pH value. When the pH was 6, the adsorption capacity and removal rate reached their peaks, which were 41.37 mg/g and 82.74%, respectively. When the pH of the solution was 2, the adsorption capacity and removal rate values were lower, at 14.84 mg/g, 14.32 mg/g, and 27.68%, respectively. When the pH reached 7, the adsorption capacity and removal rate began to decrease, indicating that the pH value has an effect on the rate of lead removal. Lead ions exist in the following forms in solutions with different pH values: Pb^{2+} , $Pb(OH)^+$, $Pb(OH)_2$, $Pb(OH)_3^-$, $Pb(OH)_4^{2-}$, $Pb_2(OH)^{3+}$, and $Pb_3(OH)_4^{2+}$ [32]. When the concentration of H^+ in the solution is too high, lead ions compete with H^+ . The higher the concentration of H^+ , the less competitive lead ions will be, meaning they become unable to combine with the active site on the surface of hydrothermal carbon. Such conditions are thus not conducive to the smooth process of adsorption. At the same time, at a higher concentration of H^+ , the functional group is protonated [33], resulting in a strong interaction between these positive charges and lead ions, which makes adsorption difficult. The literature shows that there is a trade-off between Pb^{2+} and H^+ in a solution, and a series of displacement reactions may occur on the surface of hydrothermal carbons. The specific equation is as follows:



3.2.3. Influence of the Solid–Liquid Ratio on Adsorption by Hydrothermal Carbon

The experimental conditions were as follows: an adsorption temperature of 25 °C, an initial concentration of lead ions of 50 mg/L, a concentration of phosphoric acid solution of 2 mol/L, and a solid–liquid ratio in the range of 0.5~4 g/L. The reactions were allowed to continue until the adsorption reached equilibrium. The adsorption results as a factor of the solid–liquid ratio of the modified hydrothermal carbon are shown in Figure 8.

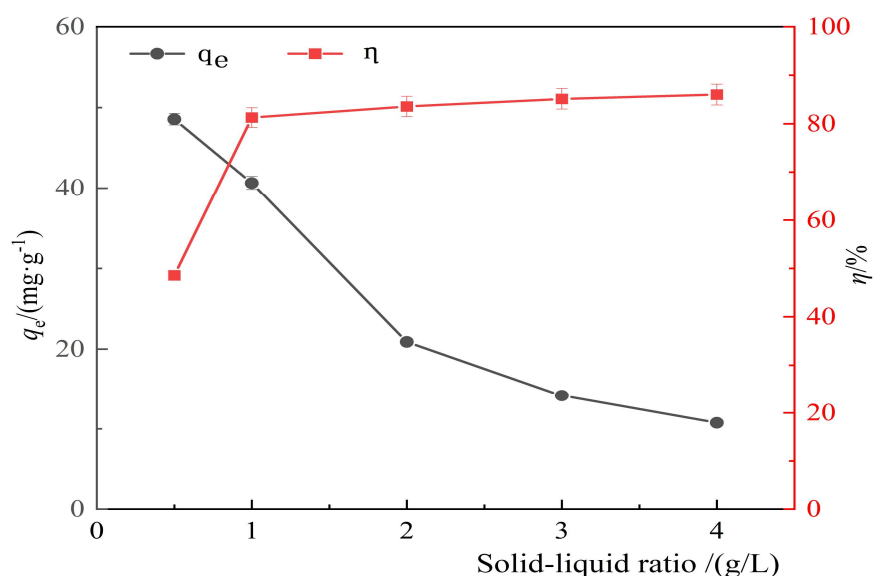


Figure 8. Effect of solid–liquid ratio on Pb(II) adsorption by hydrothermal carbon.

As can be seen from Figure 8, at a solid–liquid ratio in the range of 0.5~4 g/L, with an increase in the solid–liquid ratio, the adsorption capacity of modified hydrothermal carbon for lead gradually decreases. When the solid–liquid ratio was 0.5 g/L, the adsorption capacity was 48.56 mg/g, and when the solid–liquid ratio was 4 g/L, the adsorption capacity was 10.75 mg/g. The removal efficiency first increases and then tends to stabilize. The peak removal rate of 83.25% occurs when the solid–liquid ratio is 1 g/L. This trend is due to the rapid adsorption of lead by phosphate ions when the solid–liquid ratio is low and these ions can quickly adsorb lead. With the increase in the solid–liquid ratio, the number of active sites available for adsorption also increases; hydroxyl (–OH) and carboxyl (–COOH) come more easily into contact with Pb(II) and adsorption is enhanced. As the solid–liquid ratio continues to increase, hydrothermal carbon agglomeration occurs [34], so the active sites on the surface cannot be fully utilized. For that reason, the adsorption capacity decreases; although the removal rate of heavy metals increases, the efficiency of this system decreases.

3.2.4. Analysis of Adsorption Performance and Kinetics as Functions of Adsorption Time

The experimental conditions were as follows: an adsorption temperature of 25 °C, an initial concentration of lead ions of 50 mg/L, a solid–liquid ratio of 1 g/L, and a phosphoric acid solution concentration of 2 mol/L. The adsorption was allowed to reach equilibrium, and the adsorption time was 0–300 min. The influence of adsorption time on adsorption by modified hydrothermal carbon is shown in Figure 9.

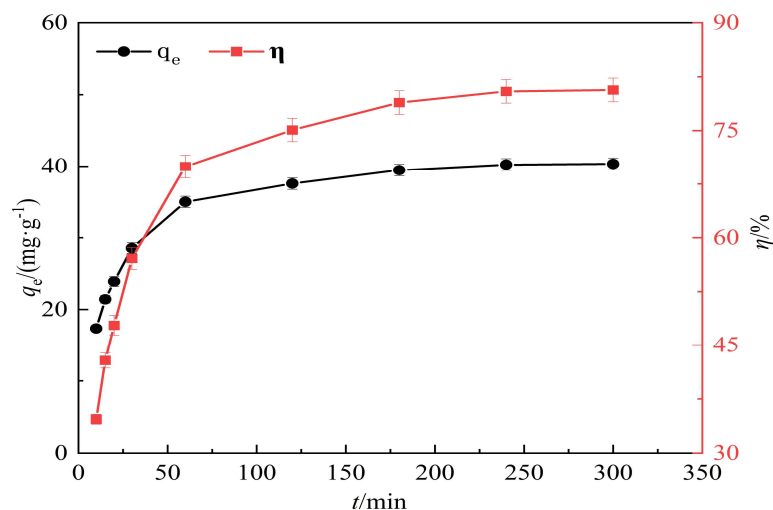


Figure 9. Effect of adsorption time on adsorption of Pb(II) by hydrothermal carbon.

As can be seen from Figure 9, with the increase in adsorption time, the adsorption capacity of modified hydrothermal carbon first increased and then tended to stabilize. After 250 min, the adsorption capacity of hydrothermal carbon for lead ions essentially stopped changing, having reached 81.66%. These results show that P-HTC adsorption occurred mainly in the first 60 min. This result is mainly due to the fact that in the initial stage of adsorption, the relative concentration of lead ions in the solution is high, there are many unoccupied active sites, and there is a high chance that the adsorbent will collide with the lead ions, making adsorption easy. After 180 min, with the decrease in the lead ion concentration and the decrease in the number of available adsorption sites on the surface of the modified hydrothermal carbon, the probability of collision is greatly reduced, reducing the rate of adsorption [35].

To analyze the changes in the water/thermal char adsorption process over time and provide evidence for the mechanism of adsorption, the first-order kinetics, the second-order kinetics, and the Elovich three models were fitted. The model formulas are shown in Equations (7)–(9). The experimental conditions were pH = 7, an adsorption time of 0–6 h, a temperature of 25 °C, a solid–liquid ratio of 1 g/L, and an initial concentration of 50 mg/L.

$$q_t = q_e \times [1 - \exp(-k_1 \times t)] \tag{7}$$

$$q_t = (k_2 \times q_e^2 \times t) / (1 + k_2 \times q_e \times t) \tag{8}$$

$$q_t = (1/\beta) \times \ln(\alpha \times \beta) + (1/\beta) \times \ln(t) \tag{9}$$

where q_t is the adsorption capacity at time t , mg/g; q_e is the equilibrium adsorption capacity, mg/g; k_1 and k_2 are the rate constants, min^{-1} ; t is the reaction time, s; and α and β are the adsorption and desorption rate constants $\text{mg}/(\text{g} \cdot \text{min}^{-2})$, respectively.

The above data were fitted using the quasi-first-order kinetics model (7), the quasi-second-order kinetics model (8), and the Elovich model (9), and the fitting results are shown in Figure 10 and Table 3.

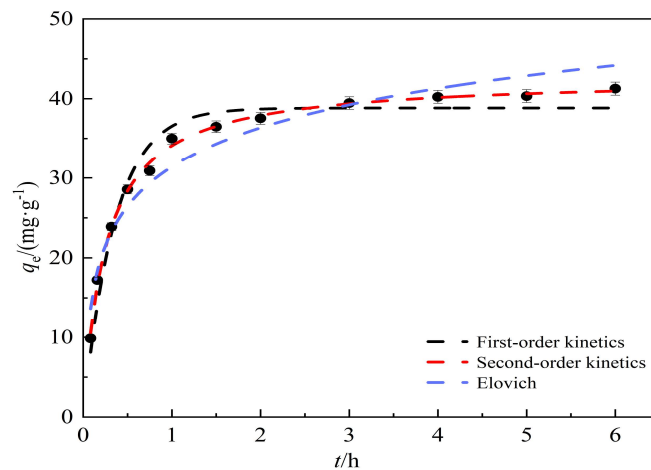


Figure 10. Kinetic analysis of adsorption by modified hydrothermal carbon.

Table 3. Table of kinetic adsorption correlation coefficient.

Adsorption Kinetic	Parameters and Correlation Coefficients			
First-order kinetics	k_1	q_e	h_0	R^2
	1/min	mg/g	mg/(min·g)	0.95
Second-order kinetics	k_2	q_e	h_0	R^2
	g/(mg·min)	mg/g	mg/(min·g)	0.99
Elovich	α	β	-	R^2
	582.59	0.14	-	0.94

As can be seen from Table 3, the three kinetic fitting models can be ranked by their coefficients of determination R^2 from low to high: the Elovich model, the quasi-first-order kinetic model, and the quasi-second-order kinetic model. The correlation coefficient R^2 reaches 0.99 in the simulation of the experimental data by the quasi-second-order kinetic model. The calculated maximum adsorption capacity of the modified hydrothermal carbon (42.68 mg/g) was close to the actual adsorption capacity (41.26 mg/g), and the relative error was 3.3%. The quasi-second-order kinetic model assumes that there is electron sharing or electron transfer between the adsorbent and the adsorbent during the adsorption process and that the adsorption rate depends mainly on chemisorption [36]. The adsorption of Pb(II) by modified hydrothermal carbon is consistent with the quasi-second-order kinetic model after fitting, which indicates that adsorption is limited by chemisorption and that the process occurs mainly by chemisorption.

3.2.5. Analysis of Isothermal Adsorption by Modified Hydrothermal Carbon

Figure 11 shows data from an experiment with an adsorption time of 120 min, an initial solution concentration of 0–500 mg/L, a solid–liquid ratio of 1 g/L, a modified phosphoric acid concentration of 2 mol/L, and the change curve of the removal rate of lead solution with different initial concentrations of modified hydrothermal carbon at different adsorption temperatures. As can be seen from the figure, with the increase in the initial concentration, the adsorption capacity of Pb(II) by the modified hydrothermal carbon increased rapidly and then stabilized, reflecting that the active sites on the surface of the effluent hot carbon changed from an unsaturated state to a saturated state and finally reached the adsorption limit and equilibrium. The adsorption capacity of hydrothermal carbon was also different at different temperatures. With the increase in temperature, the adsorption capacity of hydrothermal carbon gradually increased. It was found that the increase in temperature enhanced the Brownian motion of molecules, increased the rate

of effective collisions between Pb(II) and surface active functional groups [37], and was conducive to the molecules penetrating deeper into the internal pore structure, increasing the adsorption capacity. Thus, the increase in temperature was conducive to the adsorption. The isotherm-fitting results, combined with the kinetic-fitting results, showed that the adsorption of Pb(II) by modified hydrothermal carbon occurred by monolayer adsorption and that there were mutual repulsive forces between adsorbed Pb(II) ions. Thus, each free Pb(II) ion had to find a new active site, which became increasingly difficult, resulting in a slow increase in the adsorption rate. The final adsorption and desorption rates were the same, as the reaction reached equilibrium.

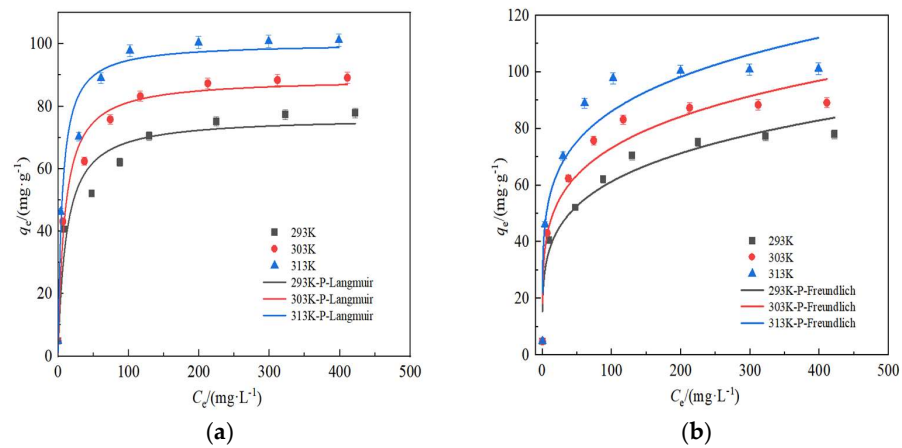


Figure 11. Thermodynamic analysis of modified hydrothermal carbon: (a) the Langmuir isotherm model; (b) the Freundlich isotherm model

As can be seen from Table 4, when the temperature was 293 K, 303 K, and 313 K, the coefficients of determination R^2 (0.94, 0.92, and 0.90, respectively) fitted by the Freundlich isotherm model were all smaller than those from the Langmuir isotherm model (0.95, 0.97, and 0.96, respectively). It can be seen that the best model fitting occurs at 303 K; below or above 303 K, the fit was lower. The fitted maximum adsorption capacity (103.24 mg/g) in the Langmuir model was closer to the actual maximum adsorption capacity (101.19 mg/g), indicating that the Langmuir model is more suitable for describing the adsorption of Pb(II) by modified hydrothermal carbon. The Langmuir model assumes that in a fixed container, the adsorption capacity per unit area of the surface of the adsorbent is the same, and only one layer of adsorbent can be adsorbed at the surface adsorption site, that is, monolayer adsorption.

Table 4. Table of sorption isotherm parameters and correlation coefficients.

Isotherm Model	Experimental Conditions	Parameters and Related Parameters		
		$K_L/L \cdot mg^{-1}$	$q_m/mg \cdot g^{-1}$	R^2
Langmuir	T/K			
	293	0.09	76.54	0.95
	303	0.11	88.94	0.97
	313	0.17	103.24	0.96
Freundlich	T/K	K_F	$1/n$	R^2
		$(mg/g(1/mg)^{1/n})$		
	293	22.46	0.22	0.94
	303	28.72	0.20	0.92
	313	35.84	0.19	0.90

3.2.6. Artificial Neural Network Model

In this study, the Neural Net Fitting module in MATLAB was used to build the artificial neural network structure, as shown in Figure 12, and the fitting results of the

P-HTC adsorption data were simulated. In the models, P-HTC refers to phosphoric acid-modified banana-skin hydrothermal charcoal. The input values were solution pH, initial concentration, oscillation time, solid–liquid ratio, and temperature for the adsorption. Corresponding to the target parameter in the table (the actual calculated value), the output values are the adsorption capacity and removal rate; corresponding to the output parameter in the table (the fitting value), the hidden layer is determined by the Kolmogorov theorem.

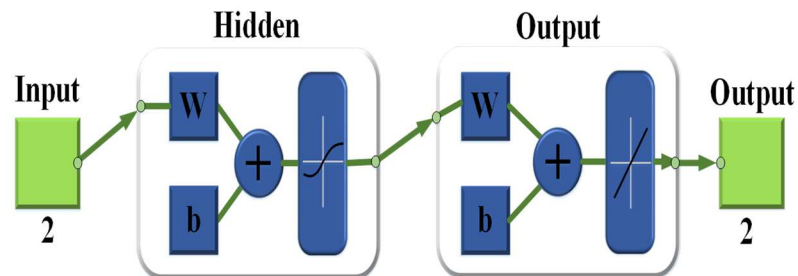


Figure 12. Structure diagram of artificial neural network.

As shown in Figure 13, solid and dotted lines represent fitted and actual values and small black circles represent input data values. The fitting results were divided into four parts. The blue line in Figure 13a represents the ANN’s data fitting; 70% of the data were input to train the model. The green line in Figure 13b represents the fitting line used to verify the training results. Input 15% data value, the red line in Figure 13c represents the fitting line of the test fitting data. Input 15% of the data value, the black lines in Figure 13d represents all of the above data fitting results.

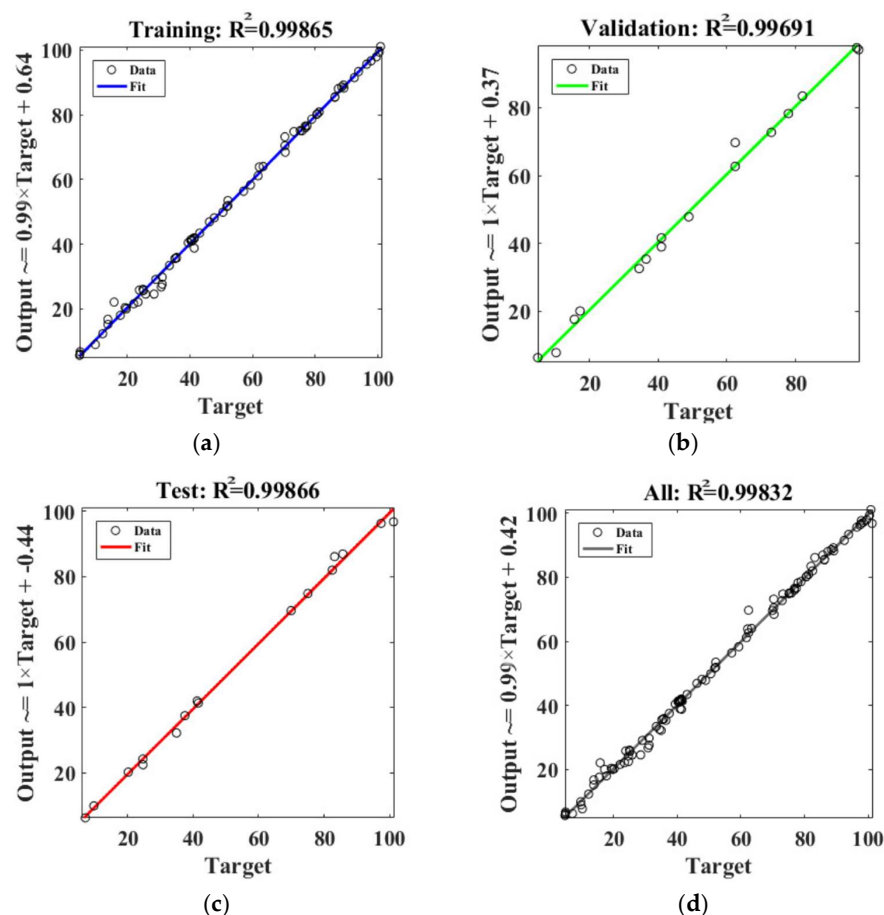


Figure 13. ANN fitting diagram of Pb(II) adsorption experimental data.

As can be seen from Figure 13, the fit of the training data, as measured by the R² value, is 0.99, as are the R² values of the models with the data used for testing and verification, indicating good fitting. After simulation in the artificial neural network, all the data were exported and saved. The module automatically generated the code that can be used to predict the adsorption capacity. Five variables were used as input values, and the code was entered into the program and run.

$$|\Delta q| = \frac{|q_F - q_e|}{|q_e|} \times 100\% \tag{10}$$

$$|\Delta \eta| = \frac{|\eta_c - \eta|}{\eta} \times 100\% \tag{11}$$

where q_F represents the adsorption capacity predicted by ANN in mg/g; q_e represents the concentration of adsorbent in solid phase at actual equilibrium in mg/g; $|\Delta q|$ represents the error between predicted adsorption capacity and actual adsorption capacity as a %; η_c —represents the removal rate predicted by ANN as a %; η represents the removal rate of actual adsorbent as a %; and $|\Delta \eta|$ represents the error between the predicted removal rate and the actual removal rate as a %.

As shown in Table 5, one of the factors is selected as a variable, and the other four factors remain unchanged. There are five factors in total, and so five conditions were tested. It can be seen that the error rates for the adsorption capacity and the removal rate are not more than 5%. There are fewer experimental datapoints for the pH and solid–liquid ratio, resulting in a larger error after training; however, the overall predicted value is close to the real value. This result shows that this method can be used to predict the adsorption, avoid repeating many experiments, gain an understanding of adsorption by hydrothermal carbon faster, and provide a theoretical reference for future applications of hydrothermal carbon in industrial designs.

Table 5. ANN prediction and actual adsorption statistics.

Input Value					Predicted Value		Actual Value		Error Value	
pH	Temperature K	Time min	Solid–Liquid Ratio g/L	Initial Concentration mg/L	q_F mg/g	η_c %	q_e mg/g	η %	$ \Delta q $ %	$ \Delta \eta $ %
2	293	120	1	50	13.1	13.2	13.8	27.6	5	4.3
7	313	120	1	50	44.4	87.8	46.2	92.4	3.8	4.9
7	293	300	1	50	40.9	80.2	40.3	80.7	1.5	0.6
7	293	120	2	50	15.23	60.4	15.8	63.4	3.6	4.8
7	293	120	1	150	74.1	24.8	75.2	25.1	1.5	1.2

3.2.7. Mechanism of Pb(II) Adsorption by Modified Hydrothermal Carbon

Figure 14 shows the mechanism of adsorption of Pb(II) by hydrothermal carbon, divided into four parts, as follows. The first mechanism is physical adsorption [38]: according to SEM images of hydrothermal carbon, there are abundant pores and fold structures on its surface. Such structures increase the van der Waals forces between molecules and enhance physical adsorption. During adsorption, the number of available surface adsorption sites decreases, and Pb(II) gradually begins to diffuse from the surface to the interior of the hole to find new adsorption sites until equilibrium is reached. The second mechanism is electrostatic attraction [39]: according to the FT-IR diagram of hydrothermal carbon, its surface contains a large number of oxygen-containing functional groups, such as $-\text{COO}^-$, $-\text{OH}^-$, $-\text{CO}^-$, and $-\text{NH}_3^+$, which are negatively charged due to deprotonation and will adsorb Pb(II) by electrostatic attraction. The third mechanism is ion exchange: the unprotonated acidic functional group and protonated delocalized π electron pair ($-\text{C}\pi\text{-H}_3\text{O}^+$) hydrogen will be replaced by Pb(II), and then H^+ will be analyzed to form polyatoms and Pb(II) ion exchange adsorption. A π - π interaction may be involved in the adsorption process, forming a π stacking structure and increasing ion exchange. The fourth mechanism is

surface complexation: according to the FT-IR diagram, the surface of hydrothermal carbon contains a large number of hydroxyl and carboxyl groups, and the lone-pair electrons of hydroxyl and carbonyl groups [40] can be shared with Pb(II) such that the ion is adsorbed onto the surface of the hydrothermal carbon.

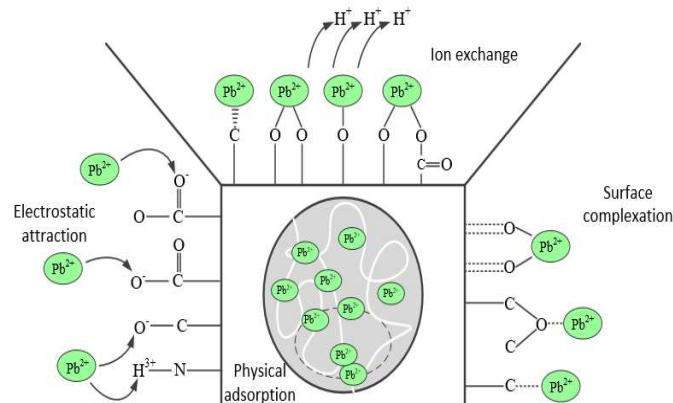


Figure 14. Schematic diagram of the mechanism of adsorption of Pb(II) by hydrothermal carbon.

3.3. The Reusability of Hydrothermal Carbon

Considering the practical applications, if the adsorption material can be used repeatedly, the cost of sewage treatment can be effectively reduced. In order to study the cyclic adsorption of Pb(II) onto hydrothermal carbon, the modified banana-peel hydrothermal carbon was dried and desorbed after it had reached saturation adsorption under the optimum adsorption conditions. Figure 15 shows the rate of Pb(II) removal for each cycle after desorption in the H₂SO₄ solution at a concentration of 0.1 mol/L. According to the figure, after five cycles, the rate of Pb(II) removal decreased slightly, from about 82.74% to 73.54%.

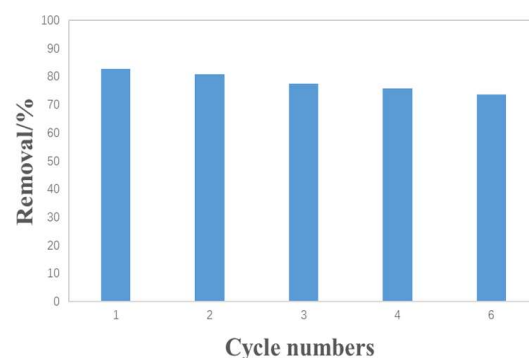


Figure 15. Efficiency of Pb(II) removal by hydrothermal carbon over five cycles.

4. Conclusions

The physicochemical properties of banana peel modified by phosphoric acid were studied using XRD, SEM, FTIR, BET, and elemental analyses. The effects of pH, adsorption time, solid–liquid ratio, and initial concentration of phosphoric acid on the adsorption of modified hydrothermal carbon were studied. The mechanism of Pb(II) adsorption by modified hydrothermal carbon was studied by means of adsorption thermodynamics and kinetics simulation. The following conclusions were drawn:

There is a large carbon sphere particle in the modified hydrothermal carbon, with a diameter of 2–3 μm; the hydrothermal material is mainly composed of amorphous carbon, and its surface contains a large number of oxygen-containing functional groups. These groups are conducive to adsorption.

The adsorption experiments carried out on hydrothermal carbon modified with different concentrations of phosphoric acid showed that the pH value, temperature, oscillation

time, and initial concentration were positively correlated with the Pb(II) adsorption capacity of hydrothermal carbon modified with different concentrations of phosphoric acid, while the increasing the solid–liquid ratio had the opposite effect.

The Langmuir model of the isotherm model is the most suitable of the tested models for describing the thermodynamic process of Pb(II) adsorption by modified hydrothermal carbon, indicating that the adsorption occurs mainly by monolayer chemisorption. Among the tested models, the quasi-second-order kinetic model best describes the kinetic adsorption of Pb(II) by hydrothermal carbon, indicating that chemical adsorption is the main process. The coefficient of determination for the artificial neural network fitting is $R^2 = 0.99$.

The mechanism of Pb(II) adsorption onto hydrothermal carbon was investigated by model fitting and characterization analysis and was found to include the following four components: physical adsorption, electrostatic attraction, ion exchange, and surface complexation. The presence of abundant pores and folded structures on the surface of the hydrothermal carbon enhances physical adsorption; the functional groups are negatively charged due to deprotonation and thus will adsorb Pb(II) by electrostatic attraction; H^+ will be resolved to form polyatoms, which will lead to Pb(II) adsorption by ion exchange; the surface of the hydrothermal carbon contains a large number of hydroxyl and carboxyl groups; and the lone pairs of electrons of the hydroxyl and carbonyl groups can be shared with Pb(II), which can thus be adsorbed on the surface of the hydrothermal carbon. The hydroxyl and carbonyl groups can share the lone-pair electrons with Pb(II) and adsorb it onto the surface of hydrothermal carbon.

Author Contributions: Designing the research methodology and writing the first draft of the paper, T.B.; Verification of the overall replication/reproducibility of results/experiments and other research outputs, Y.Y.; Make revisions to the thesis, makeup labs and tests needed for the thesis., J.Z.; Conducting a research and investigation process, specifically performing the experiments, or data/evidence collection, L.T.; Participate in the writing and revision of papers, L.Z. All authors have read and agreed to the published version of the manuscript.

Funding: This study was supported by the Shanxi Province Basic Research Program (Free Exploration) (No.202103021223031).

Data Availability Statement: Data are contained within the article.

Acknowledgments: We would like to express our gratitude to Zhiping Jin for his guidance and financial support.

Conflicts of Interest: Author Laixin Tian was employed by the company Guangdong Energy Group. The remaining authors declare that the research was conducted in the absence of any commercial or financial relationships that could be construed as a potential conflict of interest.

References

1. Zamora-Ledezma, C.; Negrete-Bolagay, D.; Figueroa, F.; Zamora-Ledezma, E.; Ni, M.; Alexis, F.; Guerrero, V.H. Heavy metal water pollution: A fresh look about hazards, novel and conventional remediation methods. *Environ. Technol. Innov.* **2021**, *22*, 101504. [[CrossRef](#)]
2. Zhu, J.B.; Zhao, J.B.; Zhou, S.P.; Wu, C.H.; Zhao, D. Study on adsorption performance and mechanism of peanut ShellBiochar for Pb^{2+} and Cd^{2+} in water. *J. Sw. Forest. Univ.* **2022**, *42*, 78–86.
3. Yao, J.; Wang, L.; Zhang, G.; Tao, J.; Shi, X.; Wei, F. Plate structure optimization and performance study of a new continuous flow electrocoagulation reactor. *Chem. Eng. Res. Des.* **2023**, *194*, 693–704. [[CrossRef](#)]
4. Madrid, F.M.G.; Arancibia-Bravo, M.P.; Sepúlveda, F.D.; Lucay, F.A.; Soliz, A.; Cáceres, L. Ultrafine Kaolinite Removal in Recycled Water from the Overflow of Thickener Using Electroflotation: A Novel Application of Saline Water Splitting in Mineral Processing. *Molecules* **2023**, *28*, 3954. [[CrossRef](#)] [[PubMed](#)]
5. Song, W.; Gao, Z.; Tan, F.; Cheng, X.; Yang, T.; Wu, D.; Yang, J.; Liang, H. Calcium sulfite oxidation activated by ferrous iron integrated with membrane filtration for removal of typical algal contaminants. *Chemosphere* **2023**, *333*, 138956. [[CrossRef](#)] [[PubMed](#)]
6. Jatoi, A.S.; Baloch, H.A.; Mazari, S.A.; Mubarak, N.M.; Sabzoi, N.; Aziz, S.; Soomro, S.A.; Abro, R.; Shah, S.F. A review on extractive fermentation via ion exchange adsorption resins opportunities, challenges, and future prospects. *Biomass Convers. Biorefin.* **2021**, *13*, 3543–3554. [[CrossRef](#)]

7. Gherbi, B.; Laouini, S.E.; Meneceur, S.; Bouafia, A.; Hemmami, H.; Tedjani, M.L.; Thiripuranathar, G.; Barhoum, A.; Mena, F. Effect of pH Value on the Bandgap Energy and Particles Size for Biosynthesis of ZnO Nanoparticles: Efficiency for Photocatalytic Adsorption of Methyl Orange. *Sustainability* **2022**, *14*, 11300. [[CrossRef](#)]
8. Vidu, R.; Matei, E.; Predescu, A.M.; Alhalaili, B.; Pantilimon, C.; Tarcea, C.; Predescu, C. Removal of Heavy Metals from Wastewaters: A Challenge from Current Treatment Methods to Nanotechnology Applications. *Toxics* **2020**, *8*, 101. [[CrossRef](#)]
9. Burakov, A.E.; Galunin, E.V.; Burakova, I.V.; Kucherova, A.E.; Agarwal, S.; Tkachev, A.G.; Gupta, V.K. Adsorption of heavy metals on conventional and nanostructured materials for wastewater treatment purposes: A review. *Ecotoxicol. Environ. Saf.* **2018**, *148*, 702–712. [[CrossRef](#)]
10. Chai, W.S.; Cheun, J.Y.; Kumar, P.S.; Mubashir, M.; Majeed, Z.; Banat, F.; Ho, S.-H.; Banat, P.L. A review on conventional and novel materials towards heavy metal adsorption in wastewater treatment application. *J. Clean. Prod.* **2021**, *296*, 126589. [[CrossRef](#)]
11. Chen, C.; Liu, G.; An, Q.; Lin, L.; Shang, Y.; Wan, C. From wasted sludge to valuable biochar by low temperature hydrothermal carbonization treatment: Insight into the surface characteristics. *J. Clean. Prod.* **2020**, *263*, 121600. [[CrossRef](#)]
12. Jagadeesh, N.; Sundaram, B. Adsorption of pollutants from wastewater by biochar: A review. *J. Hazard. Mater. Adv.* **2022**, *9*, 100226. [[CrossRef](#)]
13. González-Arias, J.; Sánchez, M.E.; Cara-Jiménez, J.; Baena-Moreno, F.M.; Zhang, Z. Hydrothermal carbonization of biomass and waste: A review. *Environ. Chem. Lett.* **2022**, *20*, 211–221. [[CrossRef](#)]
14. Barasarathi, J.; Abdullah, P.S.; Uche, E.C. Application of magnetic carbon nanocomposite from agro-waste for the removal of pollutants from water and wastewater. *Chemosphere* **2022**, *305*, 135384. [[CrossRef](#)] [[PubMed](#)]
15. Khan, T.A.; Saud, A.S.; Jamari, S.S.; Ab Rahim, M.H.; Park, J.-W.; Kim, H.-J. Hydrothermal carbonization of lignocellulosic biomass for carbon rich material preparation: A review. *Biomass Bioenergy* **2019**, *130*, 105384. [[CrossRef](#)]
16. Capobianco, L.; Di Caprio, F.; Altimari, P.; Astolfi, M.L.; Pagnanelli, F. Production of an iron-coated adsorbent for arsenic removal by hydrothermal carbonization of olive pomace: Effect of the feedwater pH. *J. Environ. Manag.* **2020**, *273*, 111164. [[CrossRef](#)]
17. Redondo-Gómez, C.; Rodríguez Quesada, M.; Vallejo Astúa, S.; Murillo Zamora, J.P.; Lopretti, M.; Vega-Baudrit, J.R. Biorefinery of Biomass of Agro-Industrial Banana Waste to Obtain High-Value Biopolymers. *Molecules* **2020**, *25*, 3829. [[CrossRef](#)]
18. Jiang, F.; Cao, D.; Hu, S.; Wang, Y.; Zhang, Y.; Huang, X.; Zhao, H.; Wu, C.; Li, J.; Ding, Y.; et al. High-pressure carbon dioxide-hydrothermal enhance yield and methylene blue adsorption performance of banana pseudo-stem activated carbon. *Bioresour. Technol.* **2022**, *354*, 127137. [[CrossRef](#)]
19. Johnson, V.E.; Liao, Q.; Jallawide, B.W., Jr.; Anaman, R.; Amanze, C.; Huang, P.; Cao, W.; Ding, C.; Shi, Y. Simultaneous removal of As (V) and Pb (II) using highly-efficient modified dehydrated biochar made from banana peel via hydrothermal synthesis. *Colloids Surf. A Physicochem. Eng. Asp.* **2023**, *663*, 131115. [[CrossRef](#)]
20. Anwar, J.; Shafique, U.; Zaman, W.U.; Salman, M.; Dar, A.; Anwar, S. Removal of Pb(II) and Cd(II) from water by adsorption on peels of banana. *Bioresour. Technol.* **2010**, *101*, 1752–1755. [[CrossRef](#)]
21. Castro, R.S.D.; Caetano, L.; Ferreira, G.; Padilha, P.M.; Saeki, M.J.; Zara, L.F.; Martines, M.A.U.; Castro, G.R. Banana Peel Applied to the Solid Phase Extraction of Copper and Lead from River Water: Preconcentration of Metal Ions with a Fruit Waste. *Ind. Eng. Chem. Res.* **2011**, *50*, 3446–3451. [[CrossRef](#)]
22. Yasim, N.S.E.M.; Ismail, Z.S.; Zaki, S.M.; Azis, M.F.A. Adsorption of Cu, As, Pb and Zn by banana trunk, Malays. *J. Anal. Sci.* **2016**, *20*, 103–112.
23. Gupta, S.; Sireesha, S.; Sreedhar, I.; Patel, C.M.; Anitha, K.L. Latest trends in heavy metal removal from wastewater by biochar based sorbents. *J. Water Process Eng.* **2020**, *38*, 101561. [[CrossRef](#)]
24. Quesada-Plata, F.; Ruiz-Rosas, R.; Morallón, E.; Cazorla-Amorós, D. Activated Carbons Prepared through H₃PO₄-Assisted Hydrothermal Carbonisation from Biomass Wastes: Porous Texture and Electrochemical Performance. *ChemPlusChem* **2016**, *81*, 1349–1359. [[CrossRef](#)]
25. Cui, Y.; Zhao, B.; Xie, F.; Zhng, X.; Zhou, A.; Wang, S.; Yue, X. Study on the preparation and feasibility of a novel adding-type biological slow-release carbon source. *J. Environ. Manag.* **2022**, *316*, 115236. [[CrossRef](#)]
26. Jiang, Q.; Xie, W.; Han, S.; Wang, Y.; Zhang, Y. Enhanced adsorption of Pb (II) onto modified hydrochar by polyethyleneimine or H₃PO₄: An analysis of surface property and interface mechanism. *Colloids Surf. A Physicochem. Eng. Asp.* **2019**, *583*, 123962. [[CrossRef](#)]
27. Pauline, A.L.; Joseph, K. Hydrothermal carbonization of organic wastes to carbonaceous solid fuel—A review of mechanisms and process parameters. *Fuel* **2020**, *279*, 118472. [[CrossRef](#)]
28. Thangarajah, V.; Wijesundara, W.M.Y.H.; Kumari, A.H.M.L.N.; Thilakarathna, M.G.G.S.N. Aqueous lead removal under optimized conditions using phosphoric acid activated coconut coir activated carbon. *Am. J. Anal. Chem.* **2020**, *11*, 389.
29. Ischia, G.; Cutillo, M.; Guella, G.; Bazzanella, N.; Cazzanelli, M.; Orlandi, M.; Miotello, A.; Fiori, L. Hydrothermal carbonization of glucose: Secondary char properties, reaction pathways, and kinetics. *Chem. Eng. J.* **2022**, *449*, 137827. [[CrossRef](#)]
30. Zikalala, S.A.; Selvaraj, R.; Al Marzouqi, F.; Kuvarega, A.T.; Mamba, B.B.; Mhlanga, S.D.; Nxumalo, E.N. Tailoring TiO₂ through N doping and incorporation of amorphous carbon nanotubes via a microwave-assisted hydrothermal method. *J. Environ. Chem. Eng.* **2020**, *8*, 104082. [[CrossRef](#)]
31. Yaashikaa, P.R.; Kumar, P.S.; Varjani, S.J.; Saravanan, A. Advances in production and application of biochar from lignocellulosic feedstocks for remediation of environmental pollutants. *Bioresour. Technol.* **2019**, *292*, 122030. [[CrossRef](#)] [[PubMed](#)]

32. Li, P.; Wang, J.; Li, X.; Zhu, W.; He, S.; Han, C.; Luo, Y.; Ma, W.; Liu, N.; Dionysiou, D.D. Facile synthesis of amino-functional large-size mesoporous silica sphere and its application for Pb²⁺ removal. *J. Hazard. Mater.* **2019**, *378*, 120664. [[CrossRef](#)] [[PubMed](#)]
33. Nair, V.; Panigrahy, A.; Vinu, R. Development of novel chitosan–lignin composites for adsorption of dyes and metal ions from wastewater. *Chem. Eng. J.* **2014**, *254*, 491–502. [[CrossRef](#)]
34. Ighalo, J.O.; Rangabhashiyam, S.; Dulta, K.; Umeh, C.T.; Iwuozor, K.O.; Aniagor, C.O.; Eshiemogie, S.O.; Iwuchukwu, F.U.; Igwegbe, C.A. Recent advances in hydrochar application for the adsorptive removal of wastewater pollutants. *Chem. Eng. Res. Des.* **2022**, *184*, 419–456. [[CrossRef](#)]
35. Fang, D.; Zhuang, X.; Huang, L.; Zhang, Q.; Shen, Q.; Jiang, L.; Xu, X.; Ji, F. Developing the new kinetics model based on the adsorption process: From fitting to comparison and prediction. *Sci. Total Environ.* **2020**, *725*, 138490. [[CrossRef](#)]
36. Aramesh, N.; Bagheri, A.R.; Bilal, M. Chitosan-based hybrid materials for adsorptive removal of dyes and underlying interaction mechanisms. *Int. J. Biol. Macromol.* **2021**, *183*, 399–422. [[CrossRef](#)]
37. Hu, S.; Huang, T.; Zhang, N.; Lei, Y.; Wang, Y. Chitosan-assisted MOFs dispersion via covalent bonding interaction toward highly efficient removal of heavy metal ions from wastewater. *Carbohydr. Polym.* **2022**, *277*, 118809. [[CrossRef](#)]
38. Khalil, A.M.E.; Memon, F.A.; Tabish, T.A.; Salmon, D.; Zhang, S.; Butler, D. Nanostructured porous graphene for efficient removal of emerging contaminants (pharmaceuticals) from water. *Chem. Eng. J.* **2020**, *398*, 125440. [[CrossRef](#)]
39. Lafi, R.; Montasser, I.; Hafiane, A. Adsorption of congo red dye from aqueous solutions by prepared activated carbon with oxygen-containing functional groups and its regeneration. *Adsorpt. Sci. Technol.* **2019**, *37*, 160–181. [[CrossRef](#)]
40. Supanchaiyamat, N.; Jetsrisuparb, K.; Knijnenburg, J.T.; Tsang, D.C.; Hunt, A.J. Lignin materials for adsorption: Current trend, perspectives and opportunities. *Bioresour. Technol.* **2019**, *272*, 570–581. [[CrossRef](#)]

Disclaimer/Publisher’s Note: The statements, opinions and data contained in all publications are solely those of the individual author(s) and contributor(s) and not of MDPI and/or the editor(s). MDPI and/or the editor(s) disclaim responsibility for any injury to people or property resulting from any ideas, methods, instructions or products referred to in the content.